Torsional Behavior of Trapezoidal and Rectangular Concrete Box-Girders Reinforced with BFRP Bars and Steel Stirrups – An Experimental Study

Mariwan Mirhaj Mohamed-Salih[1*], Ali Ramadhan Yousif[2]

1 Ph.D. student, Department of Civil Engineering, Salahaddin University-Erbil, Erbil, Iraq

[2] Professor, Department of Civil Engineering, Salahaddin University-Erbil, Erbil, Iraq

Abstract: Experimental research on hollow members under combined loading is limited due to the complex nature of the problem and the huge experimental costs involved. This study aims at examining the differences in torsional strength and stiffness, cracking pattern, and failure modes between trapezoidal and rectangular concrete box girders reinforced with longitudinal basalt fiber reinforcement polymer (BFRP) bars and steel stirrups. This unique study utilizes exclusively rectangular and trapezoidal high-strength concrete (HSC) box-girders reinforced with BFRP bars as internal longitudinal reinforcement under the combined effect of torsion, bending, and shear. Six equal size and length specimens consisting of two rectangular and four trapezoidal specimens were prepared and tested. Every specimen contains about 2.5 percent total reinforcement, equally distributed between the longitudinal BFRP bars and transverse steel stirrups. The 5 m long specimens were restrained against torsion at the supports and subjected to an eccentric load at midspan, which produces a combination of torsion, shear, and bending but with torsion as the dominant action. The study variables were the effect of shape (rectangular vs. trapezoidal), the strength of concrete (high-strength vs. normal-strength concrete), stirrup configuration, and effect of overhangs on the ultimate torsional capacity to find which variable can enhance the ultimate capacity the most (without any increase in the amount of reinforcement). The most significant finding was that the transversely stiffened specimen, B-16, was able to offer the highest torsional capacity; this is achieved without any increase in the total amount of reinforcement but with a new confinement technique in which additional one-leg stirrups act as transverse stiffeners that hold all the cage together by interconnecting internal and external legs of the stirrups to resist the twisting action as one compact unit.

Keywords: box-girder, high-strength concrete, fiber reinforcement polymer bar, torsion, combined loading.

用玄武岩纖維增強聚合物鋼筋和鋼箍筋加固的梯形和矩形混凝土箱樑的扭轉行為——一項試驗研究

摘要：由於問題的複雜性和所涉及的巨大實驗成本，在組合載荷下對空心構件的實驗研究受到限制。本研究旨在檢查用縱向玄武岩纖維增強聚合物鋼筋和鋼箍筋增強的梯形和矩形混凝土箱樑在扭轉強度和剛度、開裂模式和破壞模式方面的差異。這項獨特的研究完全利用了用玄武岩纖維增強聚合物鋼筋加固的矩形和梯形高強度混凝土箱樑作為在扭轉、彎曲和剪切的綜合作用下的內部縱向鋼筋。製備和測試由兩個矩形和四個梯形試樣組成的六個相同尺寸和長度的試樣。每個試樣包含大約 2.5% 的總鋼筋，均勻分佈在縱向玄武岩纖維增強聚合物鋼筋和橫向鋼箍筋之間。5 米長的試件在支撐處受扭轉約束，並在跨中承受偏心載荷，產生扭轉、剪切和彎曲的組合，但以扭轉為主要作用。研究變量是形狀的影響（矩形與梯形）、混凝土強度（高強度與普通強度混凝土）、箍筋配置以及懸垂對最終抗扭能力的影響，以確定哪個變量可以提高混凝土強度極限承載力最大（不增加鋼筋量）。最重要的發現是橫向加強的試樣 B-16 能夠提供最高的抗扭能力；這是在不增加鋼筋總量的情況下實現的，但採用了一

Received: June 17, 2021 / Revised: August 12, 2021 / Accepted: September 19, 2021 / Published: October 30, 2021

About the authors: Mariwan Mirhaj Mohamed-Salih, Department of Civil Engineering, Faculty of Engineering, Koya University, Koya, Iraq; Ali Ramadhan Yousif, Professor, Department of Civil Engineering, Salahaddin University-Erbil, Erbil, Iraq

Corresponding author Mariwan Mirhaj Mohamed-Salih, mariwan.mirhaj@koyauniversity.org

種新的約束技術，其中額外的單腿箍筋作為橫向加勁肋，通過將箍筋的內部和外部腿互連以抵抗扭曲作用將所有籠子保持在一起一個緊湊的單元。

关键词：箱樑、高強度混凝土、纤维增强聚合物棒、扭轉、組合荷載。

1. Introduction

Recently, fiber-reinforced polymer (FRP) bars have been introduced as a new state-of-the-art material for use in reinforced concrete structures. FRPs are reputable for their non-corrosive, light-weight, and high-tensile strength properties, and compared to steel reinforcement, FRPs offer better solutions for the problems of steel corrosion, allow for easier transportation, handling, and application, and it could be as suitable as steel for structural reinforcement [1]. However, FRPs are non-isotropic and, hence, strong only in the main longitudinal direction, which is in the direction of the reinforcing fibers. The weakness in the transverse direction affects shear strength, dowel action of FRP bars, and bond performance when used with concrete. Besides, FRPs have no plastic behavior and yield point and behave only in a linearly elastic manner up to failure; therefore, their failure is not ductile. So, if FRP fails, there will be extensive cracking together with abrupt and catastrophic failure [2]. Nanni [3] argued that there should be explicit provision to control failure by concrete crushing rather than FRP rupture regarding FRP-reinforced members. The same strategy is followed by other Codes of Practice [1, 4].

Even that torsion occurs widely when any loading deviates from the shear center of the section [5], the literature which addresses the use of FRP-reinforced members under the effect of torsion includes only a limited number of experimental researches that are carried out on solid- rectangular or spandrel FRP-reinforced beams under either pure torsion or torsion with flexure only [6-14]. To the author's knowledge, to date, there is no experimental research concerned with BFRP reinforced hollow members under the combined actions of torsion, shear, and flexure. Moreover, except for the Canadian standards [4], other design codes do not provide any provision for the torsional design of FRP-reinforced members. So there are few experimental databases and design guidelines on the behavior of FRP-reinforced hollow members under combined loadings of torsion, shear, and bending, which urges for this experimentally gap-filling research to be conducted.

To date, no research has been dealt with the performance of trapezoidal and rectangular concrete box-girders reinforced with BFRP bars and steel stirrups under torsion, shear, and moment. BFRP bars are used to assess their suitability as the main reinforcement instead of traditional steel bars. At the same time, stirrups were made of steel rather than BFRP due to higher costs in producing BFRP stirrups together with deficiencies at their bends. The current study mainly aims at examining the differences in torsional strength and stiffness, cracking pattern experimentally, and failure modes between trapezoidal and rectangular concrete (HSC) box girders reinforced with longitudinal BFRP bars and steel stirrups by assessing the effect of shape, reinforcement configuration, strength of concrete, and the effect of overhangs. These can ultimately enhance the torsional capacity, and this study revealed that the most enhanced it could be obtained with proper detailing.

2. Experimental Program

2.1. Specimen Details

Six specimens out of 25 box-girders are selected from a wide-scope Ph.D. program by the authors. The specimens are categorized into three groups. In general, all the specimens are reinforced with a total reinforcement ratio of 2.5 percent, equally divided longitudinally and transversally. Moreover, to maintain the same reinforcement area, in the single-layer reinforced specimens, 12 mm stirrups at closer spacings are used compared to 8mm stirrups at wider spacings in the double-layer reinforced specimens. As the FRP-made stirrups are inefficient due to strength decline at their bent locations [15], steel stirrups are utilized for this study.

B-23 is rectangular and designed with a constant thin-wall thickness of 120 mm, and a double layer of reinforcement is distributed all around the cross-section. B-06 is similar to B-23 and shares an equivalent concrete area to B-23, but it is trapezoidal. B-17 is similar to B-06 except that it is cast with NSC concrete. B-16 is similar to B-06, except that B-16 is reinforced with 8mm two-leg stirrups at 98mm c/c and one-leg stirrups in between, which serve as transverse stiffeners holding the outer and inner reinforcement in position. B-18 and B-19 areas are the same as B-23 and B-06 but provided with side overhangs to assess the effect of overhangs on the torsional behavior. Details of specimen cross-sections, their geometry, and reinforcement layout are as shown in Fig. 1.

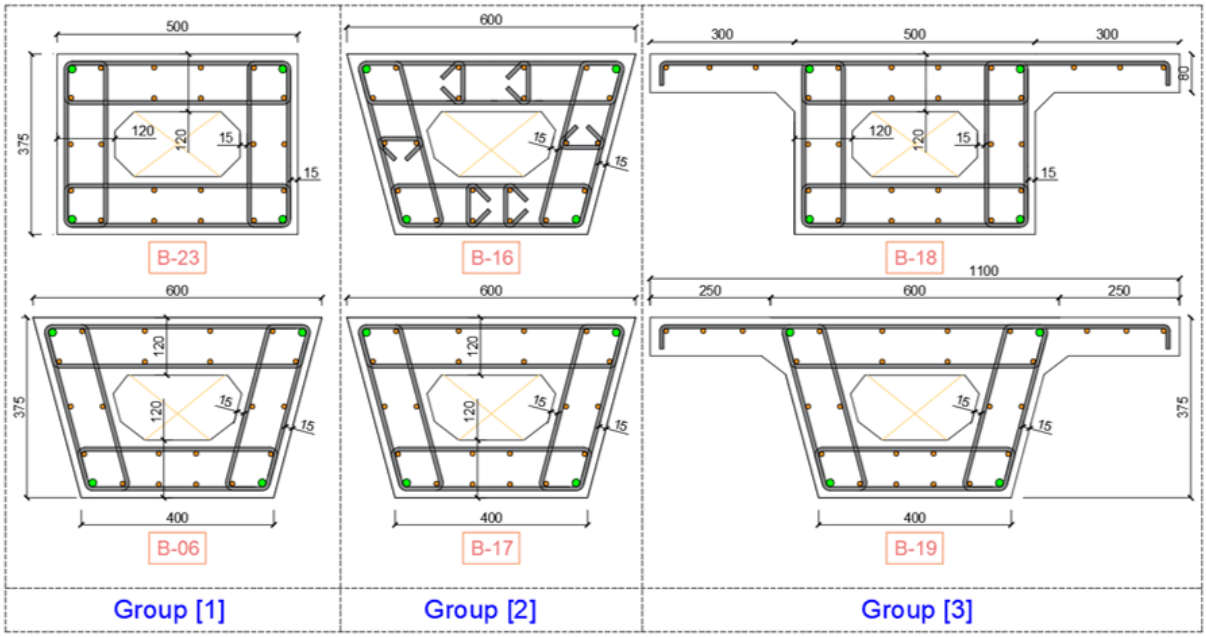

Fig. 1 Specimen dimensions and reinforcement configuration

The total length of each box-girder is 5000 mm, including two hollow parts, a central 400 mm wide solid diaphragm, and another two 450 mm wide solid diaphragms at both ends. Heavier reinforcement was utilized at the diaphragms to avoid excessive cross-sectional distortions and to minimize warpage. The hollow parts are selected as test zones, and these were 1850 mm long on each side of the middle span of the beam and formed using low-elastic polystyrene blocks.

Table *1* presents the details of the reinforcement used in each specimen.

Table 1 Properties of box-girder specimens

#	Variables	Reinforcement		S, mm	A_l, mm^2	A_t, mm^2	$\rho_l = \frac{A_l}{A_{oh}}$,%	$\rho_t = \frac{A_t \times p_h}{s \times A_{oh}}$,%
		BFRP Bars	Stirrups					
B-23	Rectangular with HSC Concrete	4Ø16 + 20Ø10	Ø08	88	2384	50	1.27	1.21
B-06	Trapezoidal with HSC Concrete	4Ø16 + 20Ø10	Ø08	88	2384	50	1.27	1.21
B-16	Trapezoidal with HSC & Stiffeners	4Ø16 + 20Ø10	Ø08	98	2384	50	1.27	1.21
B-17	Trapezoidal with NSC Concrete	4Ø16 + 20Ø10	Ø08	88	2384	50	1.27	1.21
B-18	Rectangular with Overhangs & HSC	4Ø16 + 20Ø10	Ø08	88	2384	50	1.27	1.21
B-19	Trapezoidal with Overhangs & HSC	4Ø16 + 20Ø10	Ø08	88	2384	50	1.27	1.21

After assembling the reinforcement cages as shown in Fig. 2, a total of 16 strain gauges were mounted on the longitudinal bars and stirrups at two sections: one at 50mm from the face of the midspan diaphragm and the other at 50mm from the face of one of the support diaphragms. Next, plywood molds were prepared, and then the reinforcement cages were positioned inside the molds and adjusted to get the required covers; for each hollow part, the collapsible void formers were fixed to create the required hollow core. Ready-mix concrete was then used to cast the specimens together with quality-control samples (cylinders, cubes, and prisms), and all the samples were allowed 24 hours to harden, and after that, the forms were removed. The samples, then, were kept moisturized for at least 28 days according to the ASTM standard [16]. The box-girder specimens were then painted using acrylic emulsion paint, and one of the test zones was highlighted with equal grids.

2.2. Material Properties

2.2.1. Concrete

The program uses high-strength concrete (HSC) for five of the specimens and normal strength concrete (NSC) for B-17 only. The HSC and NSC concrete were designed for a targeted 28-day cylinder compressive strength of 60 and 25 MPa.

Ошибка! Источник ссылки не найден. shows the proportions used in the mix design for the HSC concrete with a maximum size of coarse aggregate of 10 mm so that these particles could be easily accommodated within the 15 mm side covers.

Fig. 2 Reinforcement cages and mold

Table 2 HSC concrete mixture proportions

Constituents	Mix proportions, kg/m^3
	Target strength, 60 MPa
Cement	550
Sand	670
Gravel	980
Water	180
Superplasticizer, hyperplastic 200	5.5

In order to determine the concrete properties, a range of specimens from the same batches as the main box girders were prepared and tested. Samples consisting of a total of twelve cylinders (Ø100×200) mm, six (Ø150×300) mm cylinders, six (Ø150×300) mm cylinders, and a set of six (100×100×500) mm concrete prisms were prepared and tested at the age of 68-days to determine the required compressive strength, modulus of elasticity, tensile strength, and flexural strength of concrete, respectively. Table 3 shows the average values of the tested strengths at the age of 68 days, and considering time-effects, the strength values at 28-days age were re-calculated using the provisions of fib Code [17] and entered in the last column of the table for evaluation purposes. The 28-day results for the NSC concrete were 25.5 MPa, 2381 kg/m^3, 23.6 GPa, 2.30 MPa, and 4.11 MPa, as the compressive strength, density, elastic modulus, tensile strength, and flexural strength, respectively.

2.2.2. BFRP Bars and Steel Stirrups

All the BFRP bars were ordered from Chongqing Yangkai Co., China, and their data has been provided by the manufacturer in which all BFRP test results conform to the Chinese Standard GBT228 [23]. The conventional steel bars used to make the stirrups were ordered from the local market and tested as per the ASTM standard [24].

Table presents the required properties of the BFRP bars and steel stirrups. It should be noted that different codes use different limits on the yield strength of steel reinforcement to avoid brittle failure due to web concrete crushing before yielding reinforcement. The EC2 [25] limits the yield strength of torsional reinforcement to 600 MPa, whereas the ACI Code [26] limits it to a lower limit of 420 MPa.

Table 3 Properties of HSC concrete

Parameter	Test age (day)		Test
	28	68	Standard
Compressive strength, $f_c^{'}$, MPa	61	65.6	[18]
Density, kg/m3	2426	2426	[19]
Elastic modulus, GPa	38	39.5	[20]
Tensile strength, f_t, MPa	3	3.21	[21]
Flexural strength, f_b, MPa	6	6.59	[22]

Table 4 Properties of steel and BFRP bars

Bar diameter, mm	Type	f_y, MPa	ε_y, mm/mm	f_u, MPa	ε_y, mm/mm	Weight, g/m	Density, g/cm^3	E, GPa
8	Steel	600	0.0030	954	0.222	387	7.85	200
10	BFRP	-	-	1088	0.019	150	2.10	58
16	BFRP	-	-	1004	0.017	388	2.10	58

2.3. Torsion, Shear and Moment Diagrams

From a structural point of view, the applied eccentric load in this test setup will induce a simultaneous bending, shear, and torsional action. For the case of a fixed-fixed beam loaded by a point load and a concentrated torque at midspan, the corresponding shear, torsion, and bending diagrams are shown in Fig. 3. The analysis produces a (T:M: V) ratio of (1.67:1.11: 1), which is equivalent to a T:M ratio of (1.5:1). Depending on this ratio, it is predicted that mostly torsion-dominated cracking and failure modes will govern in each test.

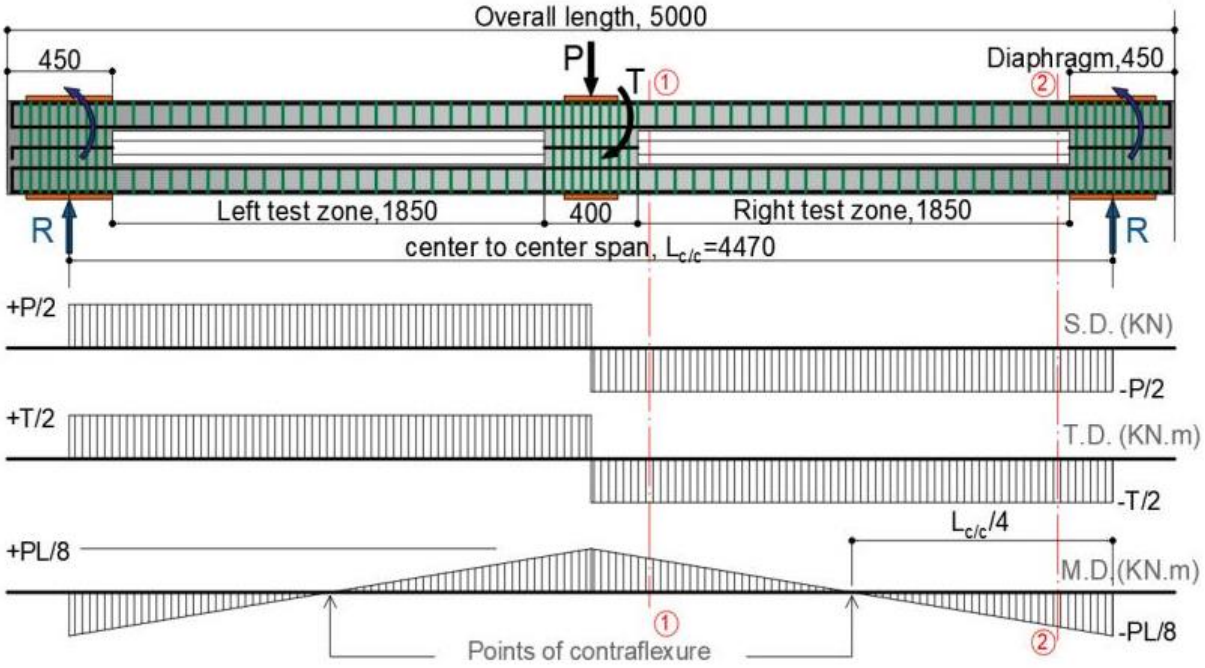

Fig. 3 Shear, torsion, and moment diagrams

2.4. Test Setup and Instrumentation

Fig. 4 presents an overview of the test setup and instrumentations for a trapezoidal box-girder with overhangs under test. All model testings were carried out at the laboratory of the Civil Engineering Department of Salahaddin University. Two new supports were constructed using welded steel frames to newly casted reinforced concrete footings. Further, two steel frames for gripping specimen ends, one steel lever arm, and two auxiliary frames for fixing instrumentations were fabricated and used to ease the conduction of the experiments. In addition, for the connections of the lever arm and support frames, strong bolts were used.

2.5. Test Procedure

Generally, the following procedure is followed in conducting all the experiments:

1) Before testing any specimen, the midspan and support frames are attached. The midspan frame provides a lever arm of 1.67 m and transfers the eccentric load from the application center-point of the machine actuator with a capacity of 2500 kN to the center of the specimens.

2) After checking the tolerances and fixing each specimen, the remaining instrumentations, including the concrete strain gauges with KPM-LVDTs, fastened to their locations.

3) An auxiliary frame independent of the rest of the test frame is used for the right test zone to provide a stable base for the operation of KTR-LVDTs. Displacement measurements are taken using a total of 16 LVDTs and considering two LVDTs for each face of the beam at each section.

4) Due to symmetry, the highlighted test zone on the left side of the specimen is utilized for the measurements related to cracks, crack propagations, the number and width of cracks.

5) The load is applied at a rate of 5 kN/min, and a compression load cell of 50-ton capacity is used to record the applied vertical loads.

6) The data from the LVDTs, load cell, and strain gauges, which produce deflection, angle of twist, concrete, and reinforcement strains, is automatically measured and recorded by the automatic 48-channel data logger. The raw data is then processed, and required relations are extracted out.

Fig. 4 General view of the test setup

3. Test Results and Discussion

Table presents the key test results, including the cracking load (P_{cr}), deflection at cracking (Δ_{cr}), ultimate load (kN), maximum deflection (Δ_u), cracking torque ($kN.m$), twist at cracking (φ_{cr}), ultimate torque ($kN.m$), and maximum twist (φ_u).

3.1. Load-Deflection Behavior

Fig. 5 shows the load-deflection responses for all the samples. Generally, the relationship is linear before and after cracking (denoted by circular marks) that could be attributed to the linear tensile response of concrete and flexural behavior mainly controlled by the longitudinal BFRP-reinforcement in each specimen. The ultimate flexural capacities range from 149 to 214 kN, and the ultimate deflections were between 21.9 to 64.55mm. In B-23, there is a shift in the position of the circular mark, indicating that the first crack occurred due to torsion but not flexure. After the flexural cracking initiates, flexural stiffness drops significantly, and nearly all the parameters in this study control the response. In Fig. 5, the circular (o), square (□), and the (×) signs represent the cracking load, yield of steel stirrups, and ultimate strain of concrete at 3000 micro-strains, respectively. As the main intention of this study is on the torsional behavior, in the next section, torsional responses will be focused on and evaluated.

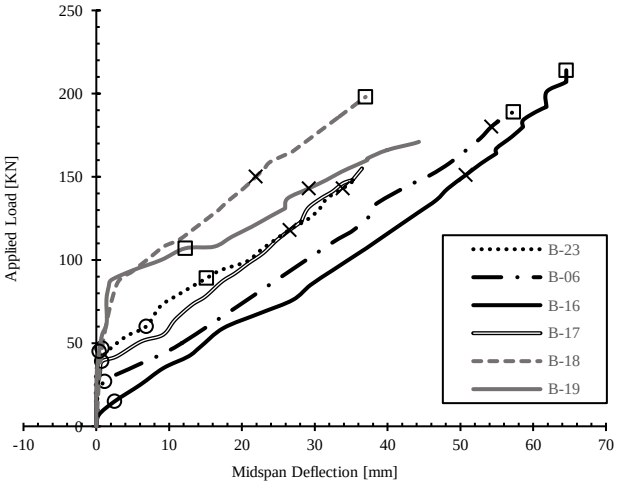

Fig. 5 Load-deflection relationships

Table 5 Principal test results

Specimens	P_{cr}, kN	Δ_{cr}, mm	P_u, kN	Δ_u, mm	T_{cr}, kN.m	φ_{cr}, rad	T_u, kN.m	φ_u, rad
B-23	60	6.85	149	35.77	100.20	0.001	248.83	0.058
B-06	27	1.14	193	58.81	45.09	0.001	322.31	0.107
B-16	15	2.52	214	64.55	25.05	0.001	357.38	0.149
B-17	39	0.77	155	36.49	65.13	0.005	258.85	0.198
B-18	47	0.80	198	36.99	78.49	0.002	330.66	0.203
B-19	45	0.39	171	44.32	75.15	0.002	285.57	0.201

3.2. Torque-Twist Response

The torque-twist curves are extracted from the data of the same LVDTs used for the load-deflection curves, as represented in Fig. 6. The symbols represent the same designations as those used for the load-deflection curves. The ultimate torsional capacities range from 248.83 to 357.38 kN.m, and the ultimate twists were between 0.058 to 0.203 radians.

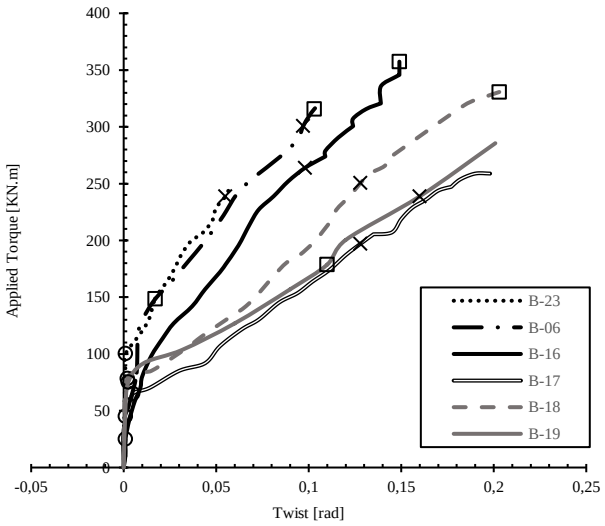

Fig. 6 Torque-twist relationships

In the following paragraphs, paired or more specimens will be compared to each other to analyze the torque-twist relationships.

Table presents the comparisons of uncracked (K_{un}) and cracked (K_{cr}) torsional stiffness for the tested specimens.

The rectangular specimen without overhangs, B-23, offers the least torsional capacity and twist angle with the highest torsional stiffness, 248.83 kN.m, 0.058 radians, and 2608 kN.m^2, respectively. The other rectangular specimen with overhangs, B-18, achieves a torsional capacity of 330.66 kN.m, higher by 33%, but with a more sacrifice for twisting, which reaches the highest value of 0.203 radians and with a considerable loss in stiffness of 1,255 kN.m2 which is about half that of B-23. These data indicate that the overhangs in rectangular specimens will effectively provide confinement to the top corners and prevent the top corners from distortions, which ultimately can provide higher resistance to the applied combined loadings. On the contrary, the side effects in rectangular box-girders with overhangs are also very significant in terms of considerable stiffness loss accompanied by higher angles of twist up to failure.

For the trapezoidal specimens with and without overhangs, B-19, and B-06, similar findings as above were obtained in all terms except torsional strength. Here, the trapezoidal specimen without overhangs, B-06, offers higher torsional capacity than its counterpart, B-19, 322.31 kN.m compared to 285.57 kN.m, respectively. However, this achievement is only about 13% which the designers can conservatively ignore. So, the overhangs in trapezoidal box-girders are not as effective as those in rectangular box-girders in improving resistance to the applied combined loadings. In B-19, there was increased twisting up to 88% compared to B-06 (0.201 vs. 0.107 radians) with a considerable loss in stiffness of 1,057 kN.m^2 which is less by about 40% compared to that of B-06. These indicated that the dowel forces could have prevented the trapezoidal box-girder with overhangs from attaining more strength, and hence a premature failure might have occurred.

The trapezoidal specimens, B-06 with HSC and B-17 with NSC concrete, demonstrate specific behavior with distinct differences between them. The ultimate torsional strength of B-06 was 322.31 kN.m which is higher than the ultimate strength of 258.85 kN.m for B-17 by about 25%. As all the other variables are unchanged, this strength development in B-06 could be attributed to the merits of using higher concrete strength with higher elastic modulus. In addition, B-06 supersedes B-17 in terms of achieving a less twist and higher torsional stiffness. The ultimate twist in B-17 was 0.198 radians (higher by 85%) than 0.107 radians in B-06. The torsional stiffness of B-17, as shown by the slope of the curve in Fig. 6 and from the calculations in

Table , is not only lower than that of B-06 but also is the lowest recorded torsional stiffness among all the specimens, which gives superior priority to the consideration of HSC for use in box-girders and other hollow structural members under the combined action of (T, V, M).

Table 6 Comparison of torsional stiffness values

B	T_{cr}, **kN.m**	φ_{cr}, **rad**	T_u, **kN.m**	$T_{u,0.85}$, **kN.m**	φ_u, **rad**	$\varphi_{u,0.85}$, **rad**	K_{un} **kN.m^2**	K_{cr} **kN.m^2**	$K_{cr,0.85}$ **kN.m^2**	$\frac{K_{un}}{K_{un(B-23)}}$	$\frac{K_{cr}}{K_{cr(B-23)}}$	$\frac{K_{cr,0.85}}{K_{cr(B-23)}}$
23	100.2	0.001	248.50	211.50	0.058	0.045	100,200	2,608	2,530	1.00	1.000	1.00
06	45.09	0.001	322.31	273.96	0.107	0.085	45,090	2,615	2,725	0.45	1.003	1.08
16	25.05	0.001	357.38	303.77	0.149	0.124	25,050	2,245	2,266	0.25	0.860	0.90
17	65.13	0.005	258.85	220.02	0.198	0.151	13,026	1,004	1,061	0.13	0.380	0.42
18	78.49	0.002	330.66	281.06	0.203	0.148	39,245	1,255	1,387	0.39	0.480	0.55
19	75.15	0.002	285.57	242.73	0.201	0.160	35,575	1,057	1,061	0.36	0.400	0.42

where K_{un} = uncracked torsional stiffness = T_{cr}/ϕ_{cr} and K_{cr} = cracked torsional stiffness = $(T_u - T_{cr})/(\varphi_u - \varphi_{cr})$

B-16, with other one-leg stirrups, which roles as transverse stiffeners connecting the outer reinforcement with the inner layer of reinforcement, offers the highest ultimate torsional capacity of 357.38 kN.m with a moderate twist of 0.149 radians. So, in a torsion-dominated scenario, the webs and flanges will be highly effective in resisting the loading if provided with outer and inner interconnected reinforcements through utilizing one-leg stirrup connectors in addition to the main two-leg stirrups surrounding the

reinforcements. These one-leg stirrups provide confinement for the longitudinal reinforcements in both the outer and inner layers, stiffen the reinforcement layers, and prevent the reinforcement from buckling due to excessive torsional twists and rotations. Eventually, such a specimen bears the largest torsional moments without increasing the amount of reinforcement. So this novel solution offers the most economical and structural sound solution among all the other scenarios.

3.3. Crack Pattern

The first cracks in the rectangular specimen without overhangs B-23 and in the over-hanged specimens B-18 and B-19 were a combination of shear and flexure cracks. They occurred at 60, 47, and 60 kN, respectively, larger than the first crack in the other specimens. These cracks were formed in both the flexural tensile zone and the shear webs concurrently and thus named "flexural-shear" cracks. Their direction was initially vertical, and then they gradually changed direction when they reached the neutral axis of the specimen. The first cracks in the trapezoidal specimens without overhangs B-06, B-16, and B-17 initiated at 12, 34, and 20 kN vertically between mid-to quarter-span, respectively, and hence named "flexural" cracks. These cracks reflect the direct effect of bending due to the lower elastic modulus of the BFRP reinforcements, which results in flexural cracks occurring first. From above, it seems evident that the first crack occurs due to normal tensile stresses, in the middle section, for insufficient tensile strength due to bending of the concrete in the lower slab, of lesser width, of the trapezoidal section. On the other case, in the sample in concrete NSC with trapezoidal section, the first crack occurs in the section with zero bending moment, due to probably insufficient resistance of the normal concrete to withstand the shear and torsional tangential stresses. Table presents the details of the first cracks.

Table 7 Details of first cracks

Beams	P_{cr}, kN	Type	Nearest position
B-23	60	Flexure-shear	Mid-Quarter span
B-06	12	Flexure	Midspan
B-16	34	Flexure	Midspan
B-17	20	Flexure	Quarter span
B-18	47	Flexure-shear	Mid-Quarter span
B-19	60	Flexure-shear	Mid-Quarter span

At every load step, the crack lines were traced and marked in the test zone. After the test, these marks were re-drawn by the AutoCAD 2D-drawing tool to better visualize the crack pattern on all faces and easily measure the angle between the cracks and the axis of the beam. Cracks on all the faces had approximate inclinations of 50, 49, 47, 46, 45, and 43 degrees for the specimens B-23, B-17, B-19, B-06, B-18, and B-16, respectively, measured clockwise from the beam axis for the left-hand test zone as is shown in Fig. 7. The average crack inclination angle is about 47 degrees which does not deviate much from the assumed 45 degrees angle specified by the ACI 318 Code [26]. Generally, more cracks formed in the webs of the flanges due to the combined action of shear, torsion, and flexural stresses leading to varied crack angles in the webs. Specimens that bear more loads show more distribution of cracks and well-formed spirals than the specimens which failed at lower loadings. Comparing the crack angles with the ultimate capacities of the specimens, it is clear that the lower the crack angle, the higher the ultimate capacity of the box-girders and vice versa and also means that compressive strut inclinations have a reverse relation with the strength of box-girders. The two specimens with overhangs, B-18, and B-19, show crack patterns and inclinations close to each other, indicating similarities in their behavior under the combined loadings. However, the crack inclination in B-18 was slightly higher than that of B-19 (45 vs. 47 degrees), and there was some spalling in B-18, which was concentrated near the midspan at the top flange. The slightly lower crack angle and spalling phenomena in B-18 could be attributed to the higher strength of B-18 as opposed to B-19. Comparing B-06 and B-17 with HSC and NSC, respectively, it can be seen that the crack pattern in the HSC box-girder is more uniform, and there are fewer widened cracks confirming that the concrete surface in the NSC box-girder is subjected to more stress than its HSC counterpart [3].

Regarding B-16, which had the highest strength, it shows the lowest average crack inclination of 43 degrees; however, the behavior was different in this specimen compared to the others as can be seen from Fig. 7 that a plastic hinge formed an axis of rotation of 61 degrees exactly midway between the support and midspan diaphragms dividing the test-zone area into two equal areas. The cracks on the left hand of the plastic deformation zone were at an average inclination of 51 degrees. In comparison, those on the right-hand area inclined at about 35 degrees, indicating that the average inclination of the cracks on both sides was 43 degrees which is the lowest crack angle amongst all. The lowest inclination of 35° on the right-hand side could also be attributed to more significant twist angles that B-16 suffers from due to its bearing to more loads before failure.

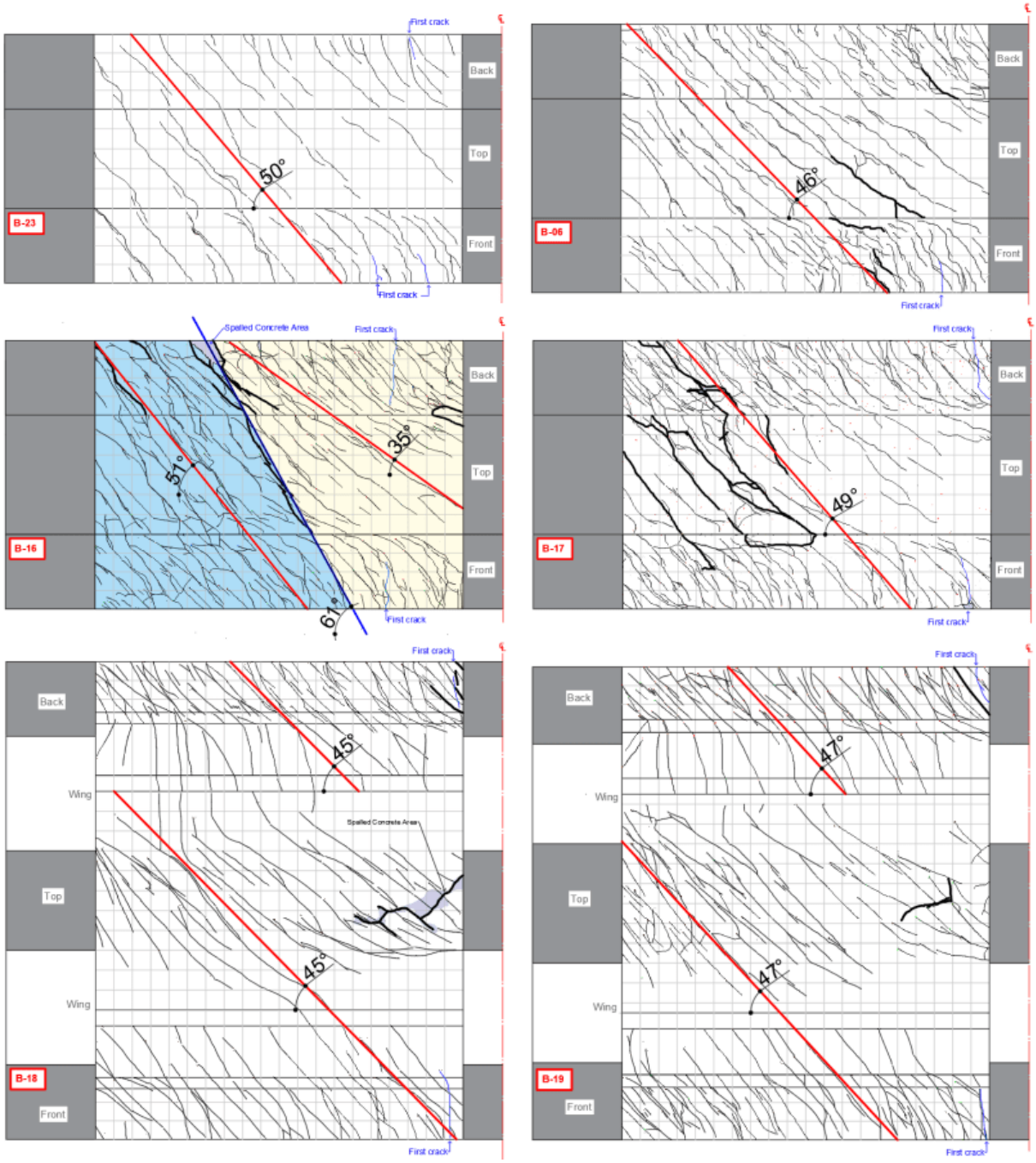

Fig. 7 Schematics of crack pattern and average strut angles

3.4. Analysis of Failure Modes

Generally, all the specimens experienced yielding of concrete and steel stirrups before failure, though the damage rate was more severe in a specific specimen than in another. The failure zone in B-23 was concentrated near the midspan due to widened cracks in the LW side. In both the trapezoidal specimens, B-06 and B-16, there were well-marked similarities in their failure modes. In both these specimens, the failure zones stuck close to the support diaphragms due to widening and crushing one of the spiral cracks, which eventually causes failure. B-17, with normal strength concrete, shows web bucking and crushing at the LW side at failure. The reason could be due to the lower strength of concrete compared to B-06 which leads to the disintegration of concrete at the LW side followed by rebar buckling and web crushing at failure. Failure modes in the specimens with overhangs, B-18 and B-19, were both at midspan due to a combination of compression failure at the top flange (which could be attributed to the addition of a grid of reinforcement for the top flange and overhangs) and shear failure due to dowel action in the BFRP re-bars close to the midspan diaphragm, as presented by Fig. 8.

Fig. 8 BFRP failure in B-19

3.5. Cross-Section Distortions

In order to study the warping effect, angular distortions at sections (1-1) and (2-2) are measured from the readings of the LVDTs attached to these sections. The final measurements are presented in Fig. 9 and Fig. 10, respectively. The angular distortions were almost in the range of ±2 degree, revealing that the closed thick BFRP-reinforced HSC box-girders stiffened with mid and support-diaphragms the effect of warping torsion could be secondary so that only circulatory torsion can be considered in the analysis. In B-16, there were larger distortions down to -3 degrees in the bottom LW corner and up to +2 degrees in the bottom UW corner that could be attributed to the highest torsional capacity of this specimen and the effect of increased loadings which it has been exposed to.

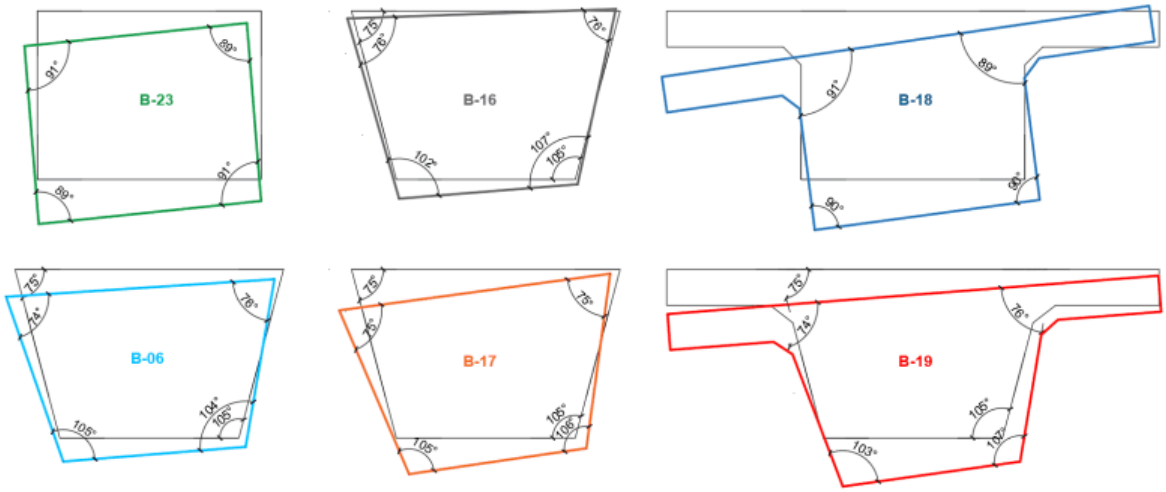

Fig. 8 Distortions at failure for section (1-1)

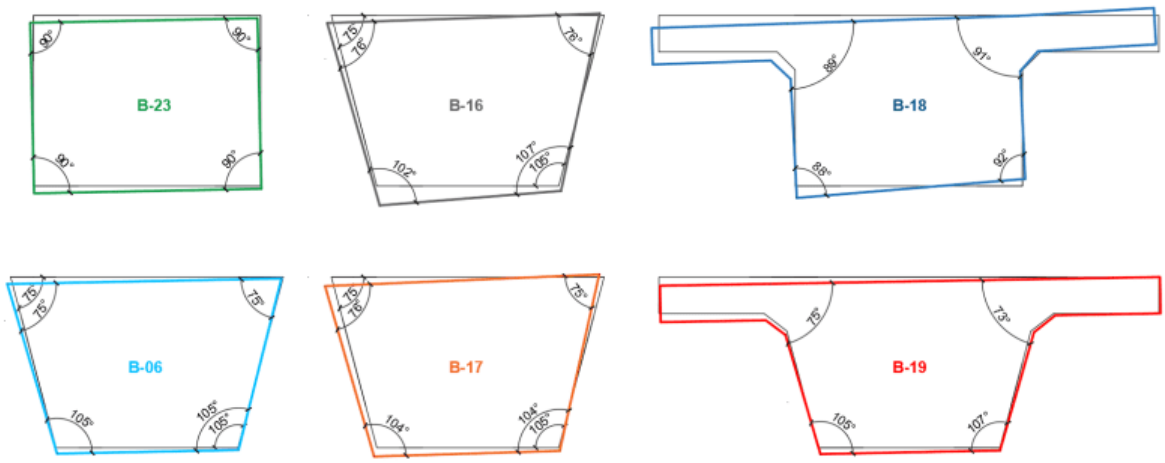

Fig. 9 Distortions at failure for section (2-2)

4. Conclusion

To date, many torsional studies mainly focus on solid concrete members reinforced with conventional steel reinforcement under pure torsion, torsion with shear, or torsion combined with flexure alone. Further, only a few types of research have addressed solid or hollow members under combined loadings using conventional steel reinforcement. FRP-related works, on the other side, focus mostly on tests of FRP-reinforced members under pure torsion. Consequently,

FRP codes of practice and design guidelines, while including provisions for the case of pure torsion, but all lack provisions regarding the torsional strength of box-girders under combined actions of torsion, shear, and bending. It is explained that FRP is a novel new-age material, but mainly because tests of specimens under combined loadings are complex, expensive, and time-consuming. At this milestone, the current research attempts to put the first steps forth towards exploring this promising area. Experimental tests on six trapezoidal and rectangular HSC box-girders (with or without overhangs) reinforced with longitudinal BFRP bars, and steel stirrups were conducted under torsion, shear, and bending. The main variables were a shape, reinforcement configuration, strength of concrete, and the effect of overhangs. The following main conclusions are drawn:

1) *Torsional behavior:* B-16, with other one-leg stirrups but with the same amount of reinforcement as the other specimens, presents the most economical and structural sound solution with the highest ultimate torsional strength of 357.38 kN.m. B-17 with NSC concrete shows the least torsional stiffness compared to its counterpart with HSC concrete, B-06. Moreover, the ultimate torsional strength increased by 25% when the compressive strength of concrete increased from 25.5 MPa in B-17 to 61 MPa in B-06. In another finding, the rectangular specimen with overhangs, B-18 achieves a torsional capacity higher by 33% than its counterpart without overhangs, B-23; on the contrary, the trapezoidal specimen without overhangs, B-06, offers a higher strength than its counterpart with overhangs, B-19. The rectangular specimen without overhangs, B-23, offers a least torsional capacity of 248.83 kN.m and the least twist of 0.058 radians but with the highest torsional stiffness compared to all other specimens.

2) *First cracks:* First cracks in the rectangular specimens with and without overhangs and in the trapezoidal box-girder with overhangs were a combination of shear and flexural cracks initiated at loadings significantly higher than those in the other specimens. On the contrary, in the trapezoidal box-girders without overhangs, the first cracks were due to flexure only and initiated at loadings much earlier than the rectangular specimen and the specimens with overhangs.

3) *Crack inclinations:* The crack angles were approximately in the range of 43 to 50 degrees with an average inclination of 47 degrees. In general, the lower the crack inclination, the more enhanced was the performance of the box-girders. B-16 with the highest strength shows an average lowest crack inclination of 43 degrees. A plastic hinge is formed midway between the midspan and support diaphragms, dividing the highlighted test zone into two equally sized areas.

4) *Failure patterns:* The specimen with NSC concrete, B-17, shows web buckling and crushing at the loaded web side at failure, which could be attributed to the use of lower strength concrete. The box-girders with overhangs both failed at midspan due to compression failure at the top flange and dowel failure in the BFRP bars near to midspan. Failure zone in the HSC rectangular specimens with and without overhangs and in the trapezoidal specimen without overhangs was due to widening spiral cracks close to the midspan and support diaphragms.

5. Limitations and Further Study

This work was limited to non-prestressed HSC box-girders subjected to torsion, shear, and bending. Further research is still needed to study the behavior of prestressed box-girders with or without overhangs (fully reinforced with FRP bars and stirrups) under the combined loading effects. Further, from the authors' viewpoint, it is also crucial that further experiments be conducted in this emerging field to supplement the FRP codes and design guidelines with a sufficient database.

Acknowledgments

The authors acknowledge the cooperation and support provided by the Concrete and Structures Lab of Salahaddin University and the Mechanics of Materials Lab of Koya University.

Notations

$f_c^{'}$ - compressive strength of concrete cylinders, MPa

f_{fu},ε_{fu} - ultimate tensile strength and strains of FRP bars;

f_y,ε_y - yield strength and strains of steel bars;

f_u,ε_u - ultimate tensile strength and strains of steel bars;

A_l , A_t - longitudinal and transverse reinf., mm^2;

ρ_l , ρ_t - longitudinal and transverse reinforcement ratio;

A_{oh} - area enclosed by the outer legs of stirrups, mm^2;

p_h - periphery enclosed by outer stirrup legs, mm;

s - center to center distance of vertical stirrups, mm;

T_{cr} - measured cracking torque of beam specimens;

φ_{cr} - measured angle of twist at cracking;

$T_{cr,0.85}$ - cracked torque at 85 percent of ultimate torque;

$\varphi_{cr,0.85}$ - angle of twist at 85 percent of ultimate torque;

T_u - measured ultimate torque of beam specimens;

φ_u - measured angle of twist at ultimate torque

References

[1] ACI440.1R-15. *Guide for the Design and Construction of Structural Concrete Reinforced with Fiber-Reinforced Polymer Bars*. American Concrete Institute, ACI Committee 440. Farmington Hills, USA, 2015.

[2] IMAD S., ODAA S.A., KAMALALDIN F.H., and JASIM M. A. Properties evaluation of fiber-reinforced polymers and their constituent materials used in structures – A review. *Materials Today: Proceedings*, 2021, 43: 1003-1008. https://doi.org/10.1016/j.matpr.2020.07.636
[3] NANNI A. Flexural behavior and design of RC members using FRP reinforcement. *Journal of Structural Engineering*, 1993, 119(11): 3344-3359. https://doi.org/10.1061/(ASCE)0733-9445(1993)119:11(3344)
[4] CAN/CSA(S-806). *Design and construction of building structures with fibre-reinforced polymers*. 2nd ed. CSA Group, Canada, 2017.
[5] AMULU C.P. & EZEAGU C.A. Combined Torsion, Bending and Shear Analysis in Reinforced Concrete. *International Journal of Advanced Trend in Technology, Management, and Applied Science*, 2016, 2(6): 45-65.
[6] DEIFALLA A., AWAD A., and ELGARHY M. Effectiveness of externally bonded CFRP strips for strengthening flanged beams under torsion: An experimental study. *Engineering Structures*, 2013, 56: 2065-2075. https://doi.org/10.1016/j.engstruct.2013.08.027
[7] KHALED S. RAGAB and AHMED S.E. Torsion Behavior of Steel Fibered High Strength Self Compacting Concrete Beams Reinforced by GFRB Bars. *International Journal of Civil, Environmental, Structural, Construction and Architectural Engineering*, 2013, 7. doi.org/10.5281/zenodo.1087620
[8] EL-AWADY E., MOHAMED HUSAIN and SAYED MANDUOR. FRP-Reinforced Concrete Beams Under Combined Torsion and Flexure. International Journal of Engineering Science and Innovative Technology (IJESIT), 2013, 2(1): 384-393
[9] SALEH A., HAMED M., DEIFALLA A., and ALI T. The effect of replacing steel reinforcements with GFRP on the torsional behavior of RC L-beams. Second Conference on Smart Monitoring, Assessment and Rehabilitation of Civil Structures, 2013.
[10] DEIFALLA A.F., HAMED M., SALEH A., and ALI T. Exploring GFRP bars as reinforcement for rectangular and L-shaped beams subjected to significant torsion: An experimental study. Engineering Structures, 2014, 59:776-786. https://doi.org/10.1016/j.engstruct.2013.11.027
[11] HAMDY M. M., CHAALLAL O. and BENMOKRANE B. Torsional moment capacity and failure mode mechanisms of concrete beams reinforced with carbon FRP bars and stirrups. *Journal of Composites for Construction*, 2015, 19(2). https://doi.org/10.1061/(ASCE)CC.1943-5614.0000515
[12] HAMDY M.M. and BENMOKRANE B. Torsion behavior of concrete beams reinforced with GFRP bars and stirrups. *Structural Journal*, 2015, 112(5):543-552.
[13] ZHOU J., SHEN W. and WANG S. Experimental Study on Torsional Behavior of FRC and ECC Beams Reinforced with GFRP Bars. *Construction and Building Materials*, 2017, 152: 74-81. https://doi.org/10.1016/j.conbuildmat.2017.06.131
[14] HADHOOD A., GOUDA M.G., AGAMY M.H., HAMDY M.M., and SHERIF A. Torsion in concrete beams reinforced with GFRP spirals. *Engineering Structures*, 2020, 206: 110174. https://doi.org/10.1016/j.engstruct.2020.110174
[15] OLLER E., MARI A., BAIRÁN J.M., and CLADERA A. Shear design of reinforced concrete beams with FRP longitudinal and transverse reinforcement. *Composites Part B: Engineering*, 2015,74: 104-122. https://doi.org/10.1016/j.compositesb.2014.12.031
[16] ASTM C31/C31M. *Standard Practice for Making and Curing Concrete Test Specimens in the Field*. ASTM International, West Conshohocken, PA, USA, 2019.
[17] INTERNATIONAL FEDERATION FOR STRUCTURAL CONCRETE. *Model Code for Concrete Structures*. International Federation for Structural Concrete, 2013.
[18] ASTM C39/C39M. *Standard Test Method for Compressive Strength of Cylindrical Concrete Specimens*. American Society for Testing and Materials, Pennsylvania, PA, 2018.
[19] ACI 363R-10. *Report on High-Strength Concrete*. American Concrete Institute. Detroit, MI, USA, 2010.
[20] ASTM C469-17. *Standard Test Method for Splitting Tensile Strength of Cylindrical Concrete Specimens*. ASTM International. West Conshohocken, PA, USA, 2017.
[21] ASTM C496/C496M. *Standard Test Method for Splitting Tensile Strength of Cylindrical Concrete Specimens*. ASTM International. West Conshohocken, PA, USA, 2017.
[22] ASTM C78/C78M. *Standard Test Method for Flexural Strength of Concrete (Using Simple Beam with Third-Point Loading)*. ASTM International. West Conshohocken, PA, USA, 2018.
[23] GB/T 228-2002. *Metallic materials – Tensile testing at ambient temperature.* Translated English of Chinese Standard. (GBT 228-2002, GB/T 228-2002, GBT 228-2002). China, 2014. https://www.chinesestandard.net.
[24] ASTM A-370. *Standard Test Methods and Definitions for Mechanical Testing of Steel Products*. ASTM International. West Conshohocken, PA, USA, 2017.
[25] EUROCODE 2. *Design of Concrete Structures, part 1: General Rules and Rules for Buildings*. Thomas Telford, London, 1992.
[26] ACI 318-19M. *Building Code Requirements for Structural Concrete and Commentary*. American Concrete Institute Committee. Farmington Hills, 318, 2019.

参考文:

[1] 交流电 I440.1R-15。用纖維增強聚合物鋼筋增強的結構混凝土的設計和施工指南。美國混凝土學會，美國混凝土協會委員會 440。美國法明頓山，2015 年。
[2] IMAD S.、ODAA S.A.、KAMALALDIN F.H. 和 JASIM M. A. 纖維增強聚合物及其結構中使用的組成材料的性能評估——綜述。今日材料：會議錄，2021 年，43：1003-1008。https://doi.org/10.1016/j.matpr.2020.07.636
[3] NANNI A. 使用玻璃鋼加固的鋼筋混凝土構件的彎曲行為和設計。結構工程雜誌, 1993, 119(11): 3344-3359。https://doi.org/10.1061/(ASCE)0733-9445(1993)119:11(3344)
[4] 能够/CSA(秒-806)。用纖維增強聚合物設計和建造建築結構。第二版。加拿大標準協會集團，加拿大，2017 年。
[5] AMULU C.P. 和 EZEAGU C.A. 鋼筋混凝土中的組合

扭轉、彎曲和剪切分析。國際技術、管理與應用科學前沿趨勢雜誌, 2016, 2(6): 45-65.
[6] DEIFALLA A.、AWAD A. 和 ELGARHY M. 外部粘合碳纖維複合材料帶用於加強受扭法蘭樑的有效性：一項實驗研究。工程結構，2013，56：2065-2075。https://doi.org/10.1016/j.engstruct.2013.08.027
[7] KHALED S. RAGAB 和 AHMED S.E. 玻璃纖維增強聚合物 鋼筋加固的鋼纖維高強度自密實混凝土樑的扭轉行為。國際土木、環境、結構、建築和建築工程雜誌，2013，7.doi.org/10.5281/zenodo.1087620
[8] EL-AWADY E.、穆罕默德·侯賽因和賽義德·曼杜爾。玻璃鋼-鋼筋混凝土梁在組合扭轉和彎曲下。國際工程科學與創新技術學報, 2013, 2(1): 384-393
[9] SALEH A., HAMED M., DEIFALLA A., 和 ALI T. 用玻璃鋼代替鋼筋對鋼筋混凝土 L 梁扭轉性能的影響。第二屆土木結構智能監測、評估和修復會議，2013。
[10] DEIFALLA A.F., HAMED M., SALEH A., 和 ALI T.。探索 玻璃鋼 鋼筋作為承受顯著扭轉的矩形和 L 形樑的鋼筋：一項實驗研究。工程結構, 2014, 59:776-786. https://doi.org/10.1016/j.engstruct.2013.11.027
[11] HAMDY M. M.、CHAALLAL O. 和 BENMOKRANE B. 用碳纖維玻璃鋼鋼筋和箍筋加固的混凝土樑的扭矩容量和破壞模式機制。建築複合材料雜誌，2015，19(2)。https://doi.org/10.1061/(ASCE)CC.1943-5614.0000515
[12] HAMDY M.M. 和 BENMOKRANE B. 用 玻璃鋼 鋼筋和箍筋加固的混凝土樑的扭轉行為。結構學報，2015，112（5）：543-552。
[13] ZHOU J., SHEN W. 和 WANG S. 玻璃鋼 鋼筋增強纖維混凝土和等等梁扭轉行為的試驗研究。建築與建築材料，2017，152：74-81。https://doi.org/10.1016/j.conbuildmat.2017.06.131
[14] HADHOOD A., GOUDA M.G., AGAMY M.H., HAMDY M.M., 和 SHERIF A. 用 玻璃鋼 螺旋加固的混凝土梁中的扭轉。工程結構，2020，206：110174。https://doi.org/10.1016/j.engstruct.2020.110174
[15] OLLER E.、MARI A.、BAIRÁN J.M. 和 CLADERA A. 具有玻璃鋼縱向和橫向鋼筋的鋼筋混凝土樑的剪切設計。複合材料乙部分：工程，2015，74：104-122。https://doi.org/10.1016/j.compositesb.2014.12.031
[16] ASTM C31/C31M。現場製作和固化混凝土試樣的標準實施規程。美國材料試驗學會國際，西康紹霍肯，賓夕法尼亞州，美國，2019 年。
[17] 國際結構混凝土聯合會。混凝土結構模型代碼。國際結構混凝土聯合會，2013 年。
[18] ASTM C39/C39 米。圓柱形混凝土試樣抗壓強度的標準試驗方法。美國測試與材料協會，賓夕法尼亞州，賓夕法尼亞州，2018 年。
[19] 国际交流协会 363R-10。高強度混凝土報告。美國混凝土學會。美國密歇根州底特律，2010 年。
[20] ASTM C469-17。圓柱形混凝土試樣劈裂抗拉強度的標準試驗方法。美國材料試驗學會 國際。美國賓夕法尼亞州西康紹霍肯，2017 年。
[21] ASTM C496/C496 米。圓柱形混凝土試樣劈裂抗拉強度的標準試驗方法。美國材料試驗學會 國際。美國賓夕法尼亞州西康紹霍肯，2017 年。
[22] ASTM C78/C78 米。混凝土抗彎強度的標準試驗方法（使用具有第三點載荷的簡單樑）。美國材料試驗學會國際。美國賓夕法尼亞州西康紹霍肯，2018 年。
[23] 国标/吨 228-2002。金屬材料 – 環境溫度下的拉伸測試。中文標準英文翻譯。（GBT 228-2002、国标/吨 228-2002 、 GBT 228-2002 ）。 中 國 ， 2014 年 。 https://www.chinesestandard.net。
[24] ASTM 一种-370。鋼產品機械試驗的標準試驗方法和定義。美國材料試驗學會 國際。美國賓夕法尼亞州西康紹霍肯，2017 年。
[25] EUROCODE 2. 混凝土結構設計，第 1 部分：一般規則和建築物規則。托馬斯·特爾福德，倫敦，1992 年。
[26] 国际交流协会 318-19 米。結構混凝土的建築規範要求和註釋。美國混凝土學會委員會。法明頓山，318，2019。